The Added Value of Diffusion Magnetic Resonance Imaging in the Diagnosis and Posttreatment Evaluation of Skull Base Chordomas

Ezgi Guler[1] Burce Ozgen[1] Melike Mut[2] Figen Soylemezoglu[3] Kader Karli Oguz[1]

[1] Department of Radiology, Hacettepe University Faculty of Medicine, Ankara, Turkey
[2] Department of Neurosurgery, Hacettepe University Faculty of Medicine, Ankara, Turkey
[3] Department of Pathology, Hacettepe University Faculty of Medicine, Ankara, Turkey

Address for correspondence Burce Ozgen, MD, Department of Radiology, Hacettepe University Faculty of Medicine, 06100 Sihhiye, Ankara, Turkey (e-mail: burce@hacettepe.edu.tr).

J Neurol Surg B 2017;78:256–265.

Abstract

Objectives To determine the use of diffusion-weighted imaging (DWI) in the pre- and posttreatment evaluation of skull base chordomas.

Design Retrospective study.

Setting Tertiary care university hospital.

Participants In total, 17 patients with histopathological diagnosis of chordoma who had magnetic resonance (MR) imaging and DWI were evaluated. Of them, 13 patients had posttreatment MR imaging including DWI.

Main Outcome Measures Three apparent diffusion coefficient (ADC) values were obtained from tumor, and an ADC value was measured from pons for the purpose of normalization. ADC values of the subtypes of chordomas (typical and chondroid chordomas) were compared.

Results Ten (59%) masses had increased signal on trace DWI at pretreatment evaluation. The mean $ADC_{entire\ tumor}/ADC_{pons}$ was calculated as 1.55 ± 0.44. The mean $ADC_{entire\ tumor}$ values of typical and chondroid chordomas were $1.26 \pm 0.29 \times 10^{-3}$ mm^2/s and $0.99 \pm 0.46 \times 10^{-3}$ mm^2/s, respectively. There was no statistically significant difference between ADC values of the subtypes ($p > 0.05$). For posttreatment evaluation, DWI enabled detection of residual tumor in the majority (85%) of cases.

Conclusions DWI is useful in diagnosis and posttreatment evaluation of skull base chordomas. However, ADC values in our series did not distinguish the subtypes of chordomas.

Keywords
- diffusion-weighted imaging
- magnetic resonance imaging
- chordoma
- skull base

Introduction

Chordomas are locally aggressive and relatively rare tumors that arise from the remnants of the embryonic notochord.[1,2] These tumors constitute approximately 1% of intracranial tumors and 4% of all primary bone tumors.[3] Intracranial chordomas account for one-third of all chordomas and most often occur in the spheno-occipital synchondrosis of

received
May 25, 2016
accepted after revision
November 20, 2016
published online
January 23, 2017

DOI https://doi.org/10.1055/s-0036-1597824.
ISSN 2193-6331.

the clivus. The site of origin may be along basisphenoid and basiocciput or unilaterally from petrous apex.[4] Other sites of intracranial origin include the sella, sphenoid sinus, nasopharynx, maxilla, paranasal sinuses, and intradural region.[5–7] Intracranial chordomas are difficult to manage on account of their critical location, local invasion, and high local recurrence rate.

Chordomas are divided into two subtypes based on microscopic morphology: typical (classic, conventional) chordomas and chondroid chordomas. Histologically, typical chordomas characteristically show large cells with vacuolated cytoplasm (physaliphorous cells) arranged in nests, cords, or sheets within a myxoid stroma.[8] They may contain areas of necrosis, hemorrhage, and entrapped bone trabeculae. Mitoses are infrequent in this subtype of chordomas. Chondroid chordomas contain areas of cartilage formation; therefore, they may resemble low-grade chondrosarcomas. These tumors can be identified with the help of immunohistochemical studies on the basis of epithelial markers that indicate their relation with notochordal mesenchyma.[9] Some reports suggest that the chondroid chordomas usually have a better prognosis,[1,10,11] whereas some demonstrate that this histopathological subtype is not associated with increased survival.[12,13]

Magnetic resonance (MR) imaging and computed tomography are used for diagnosis, treatment, and follow-up of intracranial chordomas. However, MR imaging is the best modality of choice for both pre- and posttreatment evaluation of skull base chordomas. On T1-weighted imaging (T1WI), chordomas have intermediate to low signal intensity and are easily recognized within the high signal intensity of fat of the clivus. Typical chordomas demonstrate high signal intensity on T2WI—a finding that is associated with the high fluid content of vacuolated cellular components. The majority of skull base chordomas show moderate to marked enhancement on contrast-enhanced images.[14] Chondroid chordomas have shorter T1 and T2 values compared with typical chordomas due to the replacement of watery, gelatinous matrix by cartilaginous foci.[15] However, there are no characteristic features on conventional MR imaging that may distinguish the two subtypes.[11]

In addition to conventional MR imaging sequences, diffusion-weighted imaging (DWI) is frequently used in tumor imaging. As the diffusion properties of the tissue depend on its microstructure including cellularity, nucleus/cytoplasm ratio, extracellular matrix, the DWI is known for its capability to characterize tissue in various disorders and is also helpful in the posttreatment evaluation of tumors.[16] As chordomas are surgically challenging tumors due to their location and have poor response to chemotherapy and radiation therapy, the residual tumors are frequently followed with MR imaging. However, early postoperative scans are somewhat confusing and difficult to interpret due to the lack of enhancement in many lesions and because of the presence of blood and packing materials in the surgical bed. Location of these tumors at skull base surrounded by bony structures and cerebrospinal fluid further disables accurate delineation of T2 hyperintense tumor. The purpose of this study was to determine the use of DWI in the pre- and posttreatment evaluation of skull base chordomas and to assess its use in distinguishing the subtypes.

Materials and Methods

Patients

A database search was performed to identify all patients with the histopathological diagnosis of skull base chordoma among patients who had imaging in our institution between March 2003 and May 2013. In total, 26 patients with the histopathological diagnosis of skull base chordoma were selected. Patients who underwent both conventional MR imaging and DWI were included and nine patients with inappropriate imaging (due to the lack of DWI or lack of preoperative MR imaging performed in an outside institution) were excluded. Seventeen patients were identified. According to retrospectively reviewed pathological examinations, 14 patients had typical chordoma and 3 had chondroid chordoma. Thirteen of the patients had posttreatment MR imaging including DWI. Postoperative imaging was obtained 1 to 30 days (median, 1 day) after the operation. Approval of the Institutional Review Board was obtained for this retrospective study.

Imaging

The MR imaging was performed on either a 1.5T system (Magnetom Symphony, Siemens Medical Systems, Erlangen, Germany; Achieva, Philips, the Netherlands, or Signa, GE Healthcare, Milwaukee, Wisconsin, United States) or a 3T system (Allegra, Siemens, Erlangen, Germany). Imaging protocol included axial and sagittal T1-weighted (W) spin-echo (SE), axial and coronal T2W turbo SE, axial FLAIR (fluid-attenuated inversion recovery), and axial and coronal postcontrast T1W SE imaging. The studies also included single-shot echo planar DWI (applied with *b* values of 0, 500, and 1,000 s/mm^2, TR (repetition time)/TE (echo time) of 3,500/94 ms; 5-mm slice thickness at 1.5T and TR/TE of 7,400/96 ms; 5-mm slice thickness at 3T). Apparent diffusion coefficient (ADC) maps were generated automatically using available softwares provided by the corresponding manufacturer.

Image Evaluation

A neuroradiologist (B. O.) who was blinded to the cases and who was unaware of the histopathological diagnosis randomly reviewed the preoperative and postoperative MR images including the conventional imaging and the DWI (trace and ADC images).

For the pretreatment evaluation, ADC measurements were obtained by manual outlining of a region of interest (ROI) within the tumor, excluding areas of cyst/cavity formation, hemorrhage, and necrosis, as much as possible. Three ADC values were recorded as follows: 1-ADC value of the lowest signal of tumor observed in ADC map (ADC_1) by drawing same-size uniform ROIs, 2-ADC value of the highest signal of tumor observed in ADC map (ADC_2) by drawing same-size uniform ROIs, and 3-ADC value of the entire tumor volume ($ADC_{entire\ tumor}$), detected on conventional

images by manual outlining and including the entire tumor (►**Fig. 1**).

As the normal range of ADC values from the brainstem are known from prior studies, an ADC measurement with uniform ROIs was also obtained from the pons (ADC_{pons}) as an internal quality check to assess the validity of our measurements. ADC ratios (ADC_1/ADC_{pons}, ADC_2/ADC_{pons}, $ADC_{entire\ tumor}/ADC_{pons}$) were calculated for each patient for the purposes of normalization among different magnets. The observer making the radiological evaluations noted the presence/

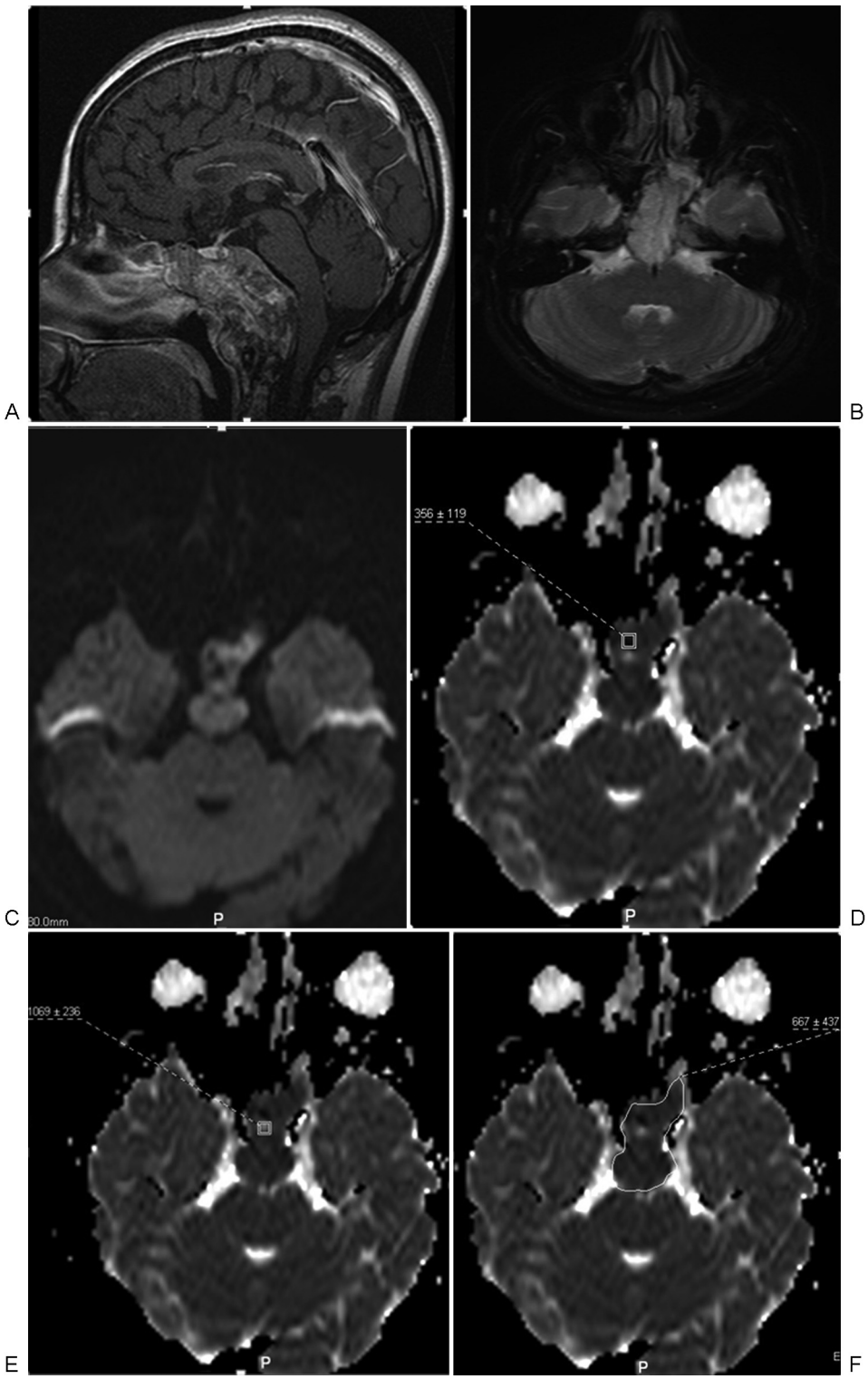

Fig. 1 (**A**) Sagittal postcontrast T1-weighted (W) image, (**B**) T2W image, and (**C**) diffusion-weighted trace image show a mass that destroys the clivus. Apparent diffusion coefficient (ADC) measurements are obtained from three locations: (**D**) ADC_1, (**E**) ADC_2, and (**F**) $ADC_{entire\ tumor}$. ADC_1, ADC value of the lowest signal of tumor observed in ADC map; ADC_2, ADC value of the highest signal of tumor observed in ADC map; $ADC_{entire\ tumor}$, ADC value of the entire tumor volume.

absence of image distortion from susceptibility artifacts on the trace DWI and especially on the ADC maps.

For the evaluation after the surgery, detectability of the residual lesion was assessed, and any signal change suggestive of recurrence was accepted as recurrent tumor. The conspicuity of the presumed residual lesion was assessed on different sequences (T2WI, FLAIR, and trace DWI scans). The assessment for the postoperative residual disease on T2WI, FLAIR, and DWI sequences was performed on a sequence-based manner, and each sequence was evaluated as a separate dataset. The three datasets were analyzed with an interval of at least 2 weeks between the readings. At each interpretation setting, the patients were presented to the reader in a random order. T1WI and postcontrast T1WI were not evaluated, as these sequences are usually difficult to assess in the early postoperative scans due to the presence of hemorrhage and packing materials. Furthermore, the variety of contrast enhancement of the chordomas also makes the assessment on postcontrast images somewhat cumbersome. Each postoperative sequence was assessed individually, with comparison to the preoperative scan. The exact location of the recurrence was not noted. The visibility of the residual tumor and the ease of its assessment was graded as follows: 0 = no appreciable residual; 1 = not well seen; 2 = detectable; 3 = conspicuous. For the patients who underwent postoperative radiation therapy, the evaluation for residual tumor was performed from imaging that was obtained after the surgery but before the radiation therapy. The final assessment of residual disease was performed with continuous clinical and imaging follow-up of the patient. The detection of residual tumors was confirmed by evaluating the follow-up MR imaging (median: 7 months; range: 1–81 months).

Histopathological Evaluation

In this study, we reviewed histopathological diagnosis of the cases. The tissue samples had been fixed in formalin and embedded in paraffin. Hematoxylin and eosin, alcian blue, toluidine blue stains and antisera for cytokeratin, S100, and epithelial membrane antigen (EMA) had been performed. Histopathologically chordomas were characterized by clusters and cords of vacuolated cells in a basophilic alcian blue positive myxoid background (►**Fig. 2A**). Tumor cells showed immunohistochemical reactivity for cytokeratin (►**Fig. 2B**), as well as S100 and EMA (►**Fig. 2C**). Cases with cartilaginous differentiation demonstrated by toluidine blue stain (►**Fig. 2D**) were diagnosed as chondroid chordoma.

Statistical Analysis

Statistical analyses were calculated with the Number Cruncher Statistical System (NCSS) 2007 Statistical Software (NCSS, Kaysville, Utah, United States). Mean, standard deviation, median, and interquartile range were used for descriptive purposes. Mann–Whitney U test was performed to detect any significant difference with respect to ADC values and ratios between the two subtypes of chordomas. Yates' corrected chi-square test was used for the comparison of qualitative data. A p-value of < 0.05 was considered significant.

Results

For the pretreatment evaluation, the study group consisted of 17 (9 female and 8 male) patients. The median age was 32 (range: 3–70) years. Histopathological diagnoses included 14 (82%) typical chordomas and 3 (18%) chondroid chordomas. Patient age and sex did not have significant difference among the groups of typical chordoma and chondroid chordoma ($p > 0.05$; ►**Table 1**).

The mean ADC values for the three locations where the measurements were obtained ($ADC_{entire\ tumor}$, ADC_1, ADC_2) and the mean ADC ratios ($ADC_{entire\ tumor}/ADC_{pons}$, ADC_1/ADC_{pons}, ADC_2/ADC_{pons},) of the whole group of chordomas and of the two subtypes are shown in ►**Table 2**. The ADC values and ratios are expressed as mean ± standard deviation and median (interquartile range). Although ADC values and ratios of typical chordomas were higher than chondroid chordomas, no statistically significant difference was detected between the two subtypes with Mann–Whitney U test ($p > 0.05$).

Three patients were excluded from posttreatment evaluation due to lack of availability of the early postoperative scans. ►**Table 3** shows the detectability of residual lesions on T2WI, FLAIR, and trace DWI scans on the postoperative scans. Eleven (85%) out of 13 residual lesions were easily recognized on trace DWI (►**Figs. 3–5**). By comparison, T2WI enabled to detect four (31%) of the residual lesions, whereas FLAIR sequences demonstrated seven (54%). When the grades of the visibility of the residual tumor were regrouped as 0 + 1 (0 = no appreciable residual; 1 = not well seen) and 2 + 3 (2 = detectable; 3 = conspicuous), there was statistically significant difference with chi-square test in distribution of detectability of residual lesions ($p = 0.021$).

Discussion

DWI is an established tool in characterizing tissue in various diseases and is also known to increase the accuracy of imaging in distinguishing malignant and benign masses.[17–20] The variation in ADC of tumors may arise from differences in cellular density, nuclear-to-cytoplasmic ratio, extracellular matrix, presence of fibrosis, and perfusion characteristics.[21,22] Lower ADC values in malignant neoplasms than their benign counterparts have been attributed to reduced water motion within cells due to high nuclear-to-cytoplasmic ratio, hypercellularity, and a reduced extracellular matrix.[18–20] In addition to the benign–malignant discrimination, the DWI may also reveal specific diffusion parameters related to the histopathological characteristics of the lesions. In our study, for the pretreatment evaluation, the mean $ADC_{entire\ tumor}$ values of chordomas as a whole group, of typical subtype, and of chondroid subtype were $1.21 \pm 0.32 \times 10^{-3}$ mm^2/s, $1.26 \pm 0.29 \times 10^{-3}$ mm^2/s, and $0.99 \pm 0.46 \times 10^{-3}$ mm^2/s, respectively. Our mean ADC value ($ADC_{entire\ tumor}$) for typical chordoma that reflected the average of 14 cases was in accordance with the value of $1.474 \pm 0.117 \times 10^{-3}$ mm^2/s reported by Yeom et al.[23] Freeze and Glastonbury[24] demonstrated a median ADC value of 1.35×10^{-3} mm^2/s (25th percentile: 1.16×10^{-3} mm^2/s; 75th percentile: 1.44×10^{-3} mm^2/s) for a sample of 14

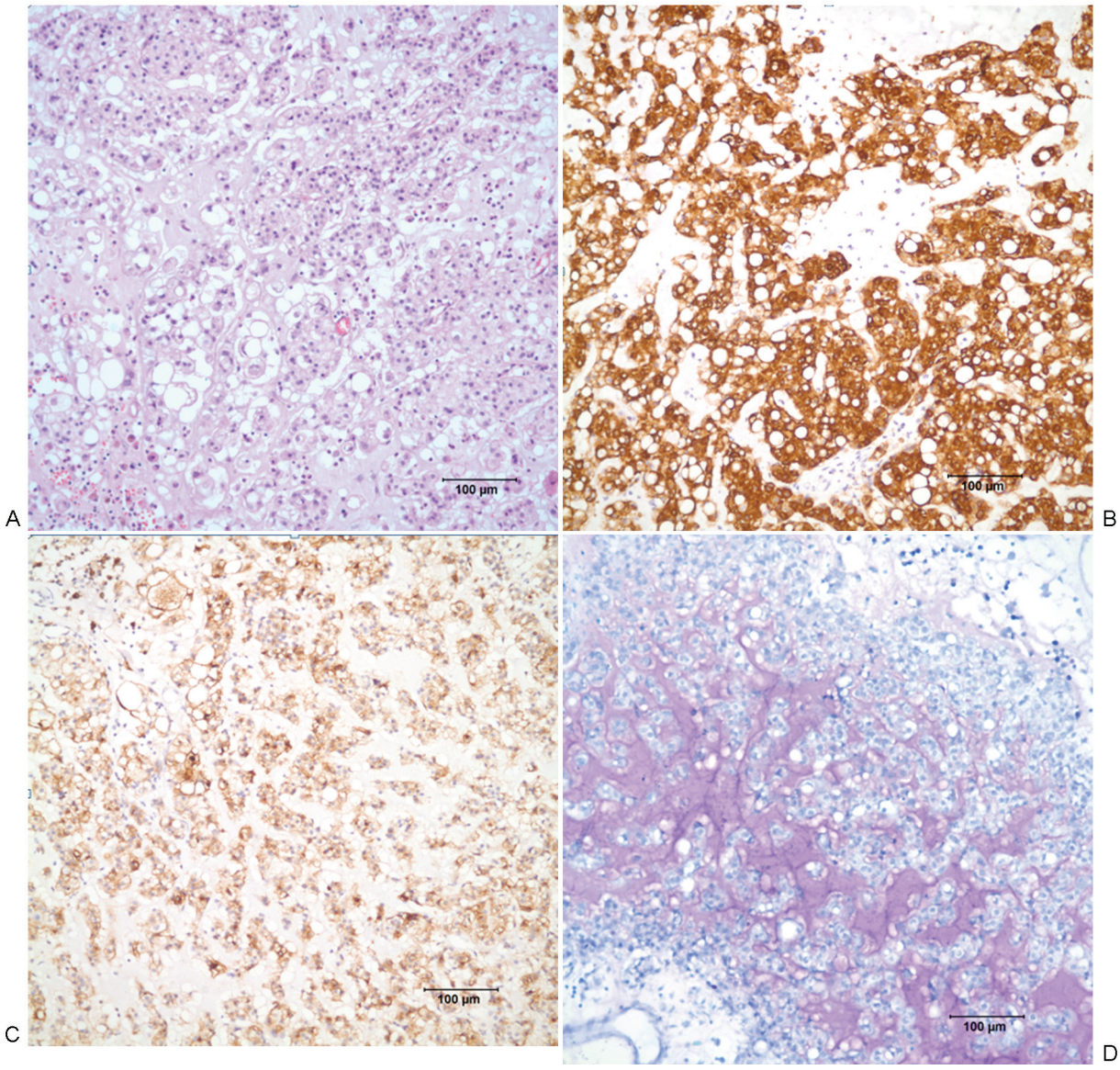

Fig. 2 Figures showing histopathological features of the chordomas. (**A**) Chordoma composed of clusters and cords of polygonal cells some showing vacuolization in a myxoid background. (**B**) Tumor cells are cytokeratin immunoreactive. (**C**) Tumor cells show immunohistochemical reactivity for epithelial membrane antigen. (**D**) Cartilaginous differentiation demonstrated by toluidine blue stain in chondroid chordoma.

Table 1 Patient characteristics for the whole group of chordomas, chondroid chordomas, and typical chordomas

		Chordoma ($n = 17$)	Typical ($n = 14$)	Chondroid ($n = 3$)	*p*-Value
Age	Mean ± SD	33.88 ± 19.93	32.64 ± 19.10	39.67 ± 27.32	0.810
	Median (IQR)	32 (15.5–52)	34 (14.5–51)	32 (17–70)	
Sex	Male	8 (47.06%)	7 (50%)	1 (33.33%)	0.601
	Female	9 (52.94%)	7 (50%)	3 (66.67%)	

Abbreviations: IQR, interquartile range; SD, standard deviation.

Table 2 ADC values and ratios obtained from three locations for the whole group of chordomas, chondroid chordomas, and typical chordomas

			Chordoma ($n = 17$)	Typical ($n = 14$)	Chondroid ($n = 3$)	p-Value
ADC (10^{-3} mm^2/s)	$ADC_{entire\ tumor}$	Mean ± SD	1.21 ± 0.32	1.26 ± 0.29	0.99 ± 0.46	0.548
		Median (IQR)	1.2 (0.94–1.5)	1.3 (1–1.51)	0.92 (0.58–1.49)	
	ADC_1	Mean ± SD	0.96 ± 0.23	0.99 ± 0.20	0.80 ± 0.33	0.993
		Median (IQR)	0.97 (0.78–1.15)	0.99 (0.84–1.14)	0.74 (0.5–1.15)	
	ADC_2	Mean ± SD	1.56 ± 0.33	1.62 ± 0.30	1.26 ± 0.35	0.998
		Median (IQR)	1.55 (1.3–1.74)	1.58 (1.38–1.82)	1.1 (1.02–1.66)	
ADC_{tumor}/ADC_{pons}	$ADC_{entire\ tumor}$	Mean ± SD	1.55 ± 0.44	1.62 ± 0.41	1.22 ± 0.52	0.611
		Median (IQR)	1.69 (1.17–1.84)	1.75 (1.36–1.88)	1.02 (0.84–1.81)	
	ADC_1	Mean ± SD	1.24 ± 0.36	1.30 ± 0.35	0.99 ± 0.37	0.914
		Median (IQR)	1.2 (0.92–1.5)	1.29 (1–1.56)	0.88 (0.68–1.4)	
	ADC_2	Mean ± SD	1.99 ± 0.54	2.08 ± 0.52	1.63 ± 0.61	0.714
		Median (IQR)	1.96 (1.82–2.29)	1.97 (1.83–2.37)	1.93 (0.93–2.02)	

Abbreviations: ADC, apparent diffusion coefficient; ADC_1, ADC value of the lowest signal of tumor observed in ADC map; ADC_2, ADC value of the highest signal of tumor observed in ADC map; $ADC_{entire\ tumor}$, ADC value of the entire tumor volume; IQR, interquartile range; SD, standard deviation.

chordoma patients without a separation to subtypes, which was similar to our findings.

When the two subtypes of chordomas were compared, both mean ADC values and ADC values relative to the pons of chondroid chordoma cases were lower than those of typical chordoma cases. However, there was no statistically significant difference, and ADC values did not distinguish the two subtypes. It was thought that this might be related to the small sample size of chondroid chordoma cases. Similarly, in a recent study in which ADC values of typical chordoma and poorly differentiated chordoma were compared, no significant difference was found between the two groups.[23] The results of previous studies suggest that DWI and calculation of ADC values may aid in distinguishing chordoma from other skull base tumors, especially chondrosarcoma.[23–25] It is thought that the myxoid stroma of chordomas impedes extracellular water motion; therefore, their ADC values are lower than those of chondrosarcomas.[23] However, diffusion characteristics of typical and chondroid subtypes are not clearly demonstrated. Chondroid chordomas may have stromal features that resemble the hyaline cartilage seen in chondrosarcoma.[1] This may result in overlapping of diffusion characteristics among these tumors. Preoperative distinction of chordoma subtypes is useful in radiological–pathological correlation. In a recent study, it was suggested that the younger patients with chondroid type skull base chordoma treated with both surgery and radiation therapy might have lower tumor recurrence rate. Therefore, distinguishing the subtypes of chordoma can have prognostic implications for the survival.[26]

DWI has been commonly applied for evaluating skull lesions and it was found to increase the conspicuity of skull tumors compared with conventional MR imaging sequences.[17] Similarly, in our study, DWI increased the visibility of lesions as 10 (59%) of them showed high signal intensity on DWI. An interesting finding of our study revealed that T2WI was not as helpful as DWI in suggesting residual tumor at posttreatment evaluation. Only 4 (31%) of 13 lesions were detectable or conspicuous on T2WI. FLAIR sequences were relatively better in delineating residual tumor, as seven (41%)

Table 3 MR imaging features at postoperative evaluation

	Detectability of residual chordomas ($n = 13$)			
	No appreciable residual (0)	Not well seen (1)	Detectable (2)	Conspicuous (3)
T2WI	1 (8%)	8 (61%)	3 (23%)	1 (8%)
FLAIR	0 (0%)	6 (46%)	7 (54%)	0 (0%)
DWI	0 (0%)	2 (15%)	8 (61%)	3 (23%)

Abbreviations: DWI, diffusion-weighted imaging; FLAIR, fluid-attenuated inversion recovery; MR. magnetic resonance; T2WI, T2-weighted imaging.

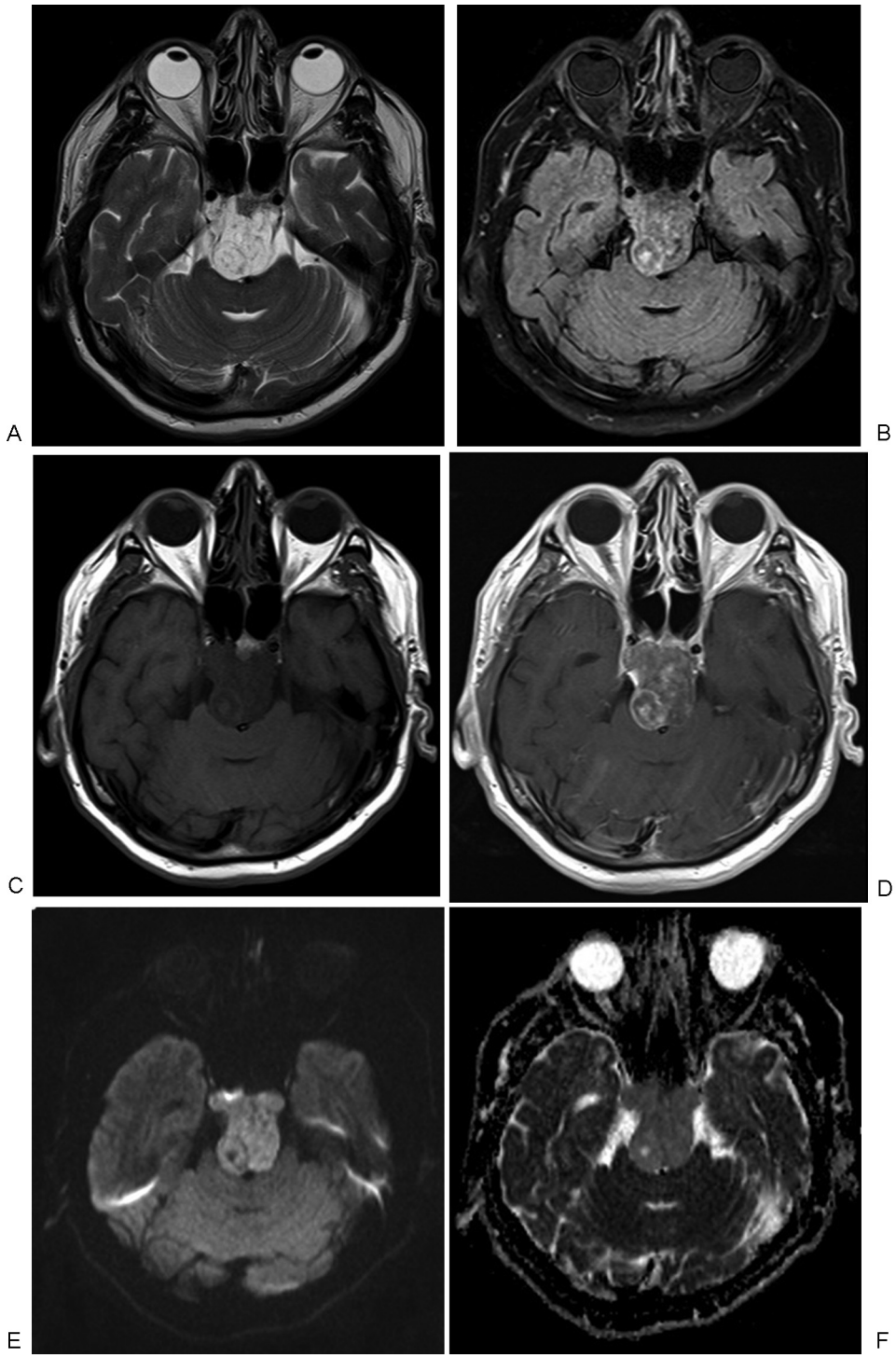

Fig. 3 Preoperative magnetic resonance images of a 40-year-old male with typical chordoma. (**A**) Axial T2-weighted (W) image and (**B**) fluid-attenuated inversion recovery image show a high signal intensity clival mass arising from the clivus, expanding prepontine cistern, and compressing the pons. (**C**) Axial T1W image and (**D**) postcontrast T1W image show that the mass enhances in a mild heterogeneous pattern. The mass is very well delineated on the diffusion-weighted trace image (**E**) and on the corresponding apparent diffusion coefficient map (F).

of the lesions were detectable. Trace DWI scans enabled to detect residual tumor better than T2 or FLAIR sequences as it provided an increased visibility of 11 (65%) lesions. This finding is of significant value, especially in the early postoperative period, to make a correct assessment regarding the residual tumor with important implications regarding the follow-up and patient counseling.

There were several limitations to our study. It was a pilot study and the small number of patients, especially for the chondroid chordoma subtype, was a major limitation. Although there was no statistically significant difference between the ADC values of the two subtypes in our study, studies with larger cohort are needed to validate the results.

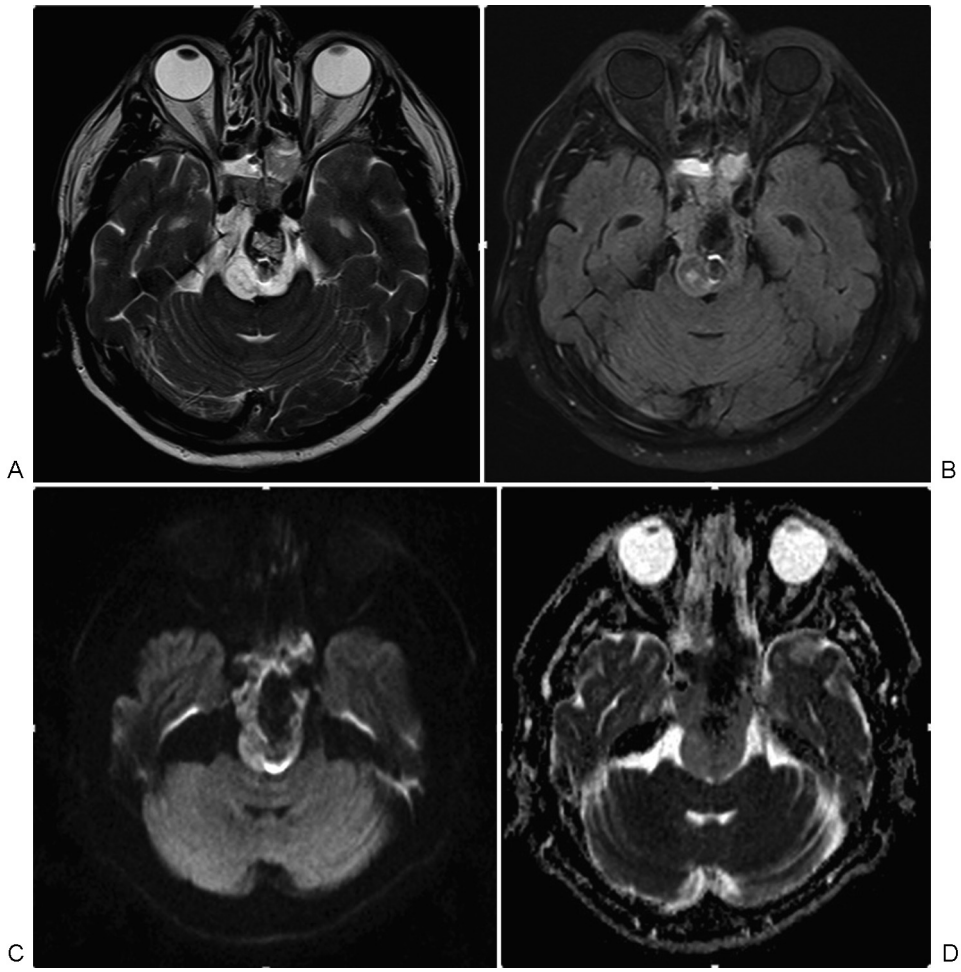

Fig. 4 Postoperative magnetic resonance images of the same patient in ►**Fig. 3**. The mass is partially resected and a residual tumor with high signal intensity in axial T2-weighted image (**A**) and intermediate signal intensity in axial fluid-attenuated inversion recovery image (**B**) is seen with evidence of hemorrhage centrally. Diffusion-weighted trace image (**C**) and corresponding apparent diffusion coefficient map (**D**) reveal a better demarcation of the residual tumor. Note slight artifacts in the resection cavity caused by surgical materials and hemorrhage.

The cystic/necrotic components and areas of hemorrhage were avoided in ROI placement' however, chordomas are known to be heterogeneous tumors, and in some lesions, myxoid stromal component may be more prominent than the physaliphorous cell component. In such an instance, although the histopathological diagnosis remains the same, the prominence of this myxoid stroma reflects in an altered overall ADC measurement and could only be accurately represented with ADC histograms, which were not performed in this study. ADC histograms of the entire tumor volume are known to better reflect internal tumor architecture and might give a better picture of the subtype analysis; however, mean ADC values and visual assessment are much more practical in routine diagnostic assessment of tumors. Additionally, the scans of different cases were performed on different MR imaging scanners, which might have affected the ADC values. To avoid the effects of the use of various magnets, we measured ADC values of the pons for the purpose of normalization and calculated ADC ratios. Comparable results of ADC ratios obtained from each scanner support our belief that the use of various scanners is not a major limitation.

Another limitation was that the posttreatment evaluation of DWI was done in a subjective manner, which was partly due to artifacts that originated from surgical materials, hemorrhage, and calcifications. The susceptibility artifacts on the DWI and especially on the ADC maps were present in five (38%) patients. A single observer evaluation of the imaging was another limitation of the study, and although care was taken to separately assess the value of different sequences, the limited number of patients might have resulted in interpretation biases.

Conclusions

DWI is useful in diagnosis and posttreatment evaluation of skull base chordomas. There are no characteristic features on conventional MR imaging to separate typical chordomas from chondroid chordomas, and ADC values failed to be helpful in distinguishing the two histopathological subtypes. However, DWI was found to be more helpful than conventional sequences for the assessment of residual tumor. Therefore, DWI should be included in the imaging protocol and thoroughly evaluated in the assessment of postoperative residual lesions of chordomas.

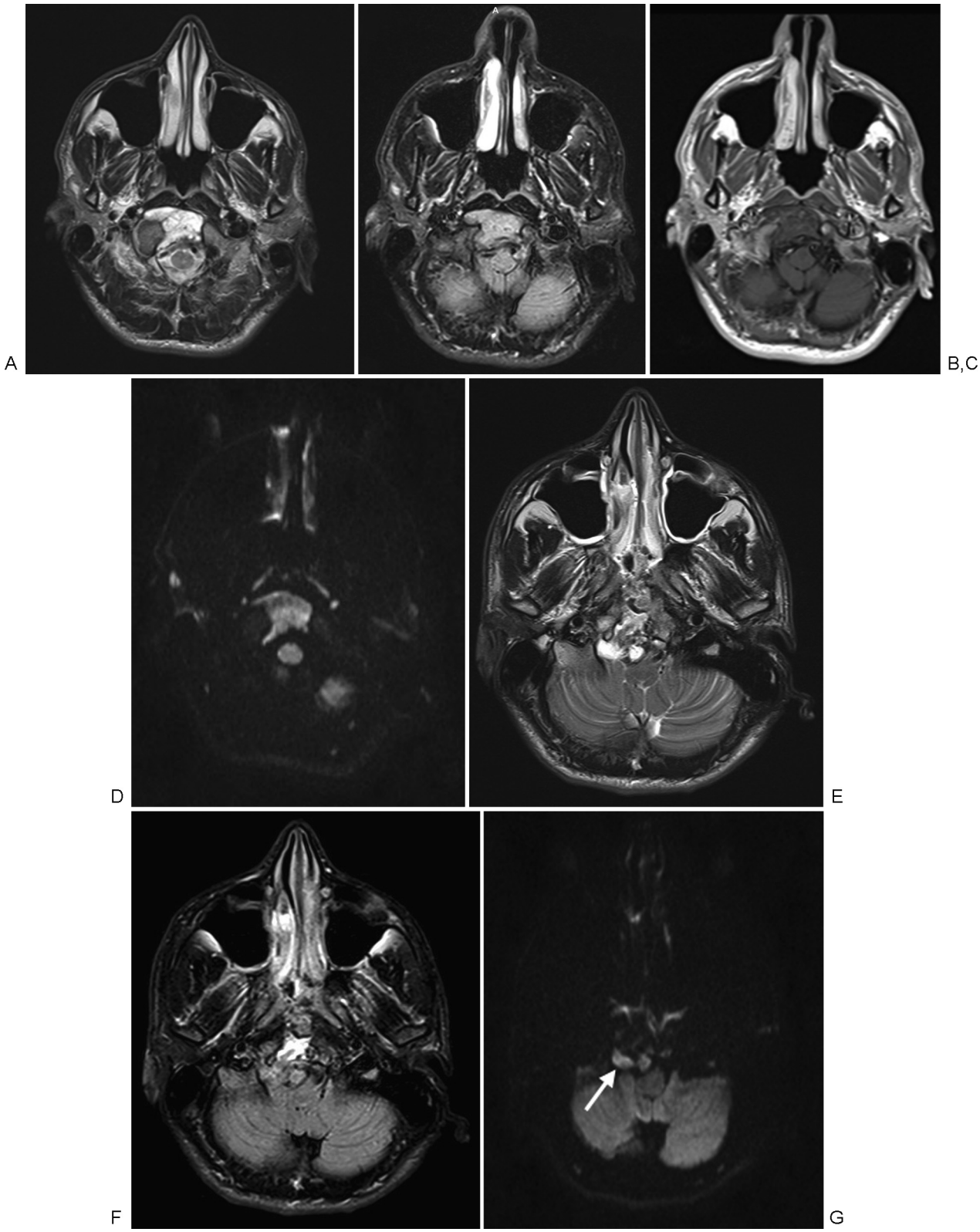

Fig. 5 (**A–D**) Preoperative and (**E–G**) postoperative magnetic resonance images of a 19-year-old male with typical chordoma. (**A**) Axial T2-weighted (W) and (**B**) axial fluid-attenuated inversion recovery (FLAIR) images show a multiseptate mass located at the inferior of the clivus. Axial postcontrast T1W image (**C**) reveals that the mass has little/no enhancement but is well defined on diffusion-weighted (DW) trace image (**D**). On the postoperative scan, the residual lesion is much easier to detect on the DW trace image (**G**) (arrow) than on the T2W (**E**) and FLAIR (**F**) images.

References

1 Heffelfinger MJ, Dahlin DC, MacCarty CS, Beabout JW. Chordomas and cartilaginous tumors at the skull base. Cancer 1973;32(2):410–420
2 Soo MY. Chordoma: review of clinicoradiological features and factors affecting survival. Australas Radiol 2001;45(4):427–434
3 Dahlin DC, MacCarty CS. Chordoma. Cancer 1952;5(6):1170–1178
4 Kendall BE. Cranial chordomas. Br J Radiol 1977;50(598):687–698
5 Ormerod R. A case of chordoma presenting in the nasopharynx. J Laryngol Otol 1960;74:245–254
6 Shugar JM, Som PM, Krespi YP, Arnold LM, Som ML. Primary chordoma of the maxillary sinus. Laryngoscope 1980;90(11 Pt 1):1825–1830
7 Mapstone TB, Kaufman B, Ratcheson RA. Intradural chordoma without bone involvement: nuclear magnetic resonance (NMR) appearance. Case report. J Neurosurg 1983;59(3):535–537
8 Mindell ER. Chordoma. J Bone Joint Surg Am 1981;63(3):501–505
9 Mizerny BR, Kost KM. Chordoma of the cranial base: the McGill experience. J Otolaryngol 1995;24(1):14–19
10 Clark WC, Robertson JH, Lara R. Chondroid chordoma. Case report. J Neurosurg 1982;57(6):842–845
11 Tsutsumi S, Akiba C, Suzuki T, et al. Skull base chondroid chordoma: atypical case manifesting as intratumoral hemorrhage and literature review. Clin Neuroradiol 2014;24(4):313–320
12 Colli BO, Al-Mefty O. Chordomas of the skull base: follow-up review and prognostic factors. Neurosurg Focus 2001;10(3):E1
13 Jian BJ, Bloch OG, Yang I, Han SJ, Aranda D, Parsa AT. A comprehensive analysis of intracranial chordoma and survival: a systematic review. Br J Neurosurg 2011;25(4):446–453
14 Erdem E, Angtuaco EC, Van Hemert R, Park JS, Al-Mefty O. Comprehensive review of intracranial chordoma. Radiographics 2003;23(4):995–1009
15 Sze G, Uichanco LS III, Brant-Zawadzki MN, et al. Chordomas: MR imaging. Radiology 1988;166(1 Pt 1):187–191
16 Bammer R. Basic principles of diffusion-weighted imaging. Eur J Radiol 2003;45(3):169–184
17 Nemeth AJ, Henson JW, Mullins ME, Gonzalez RG, Schaefer PW. Improved detection of skull metastasis with diffusion-weighted MR imaging. AJNR Am J Neuroradiol 2007;28(6):1088–1092
18 Abdel Razek A, Mossad A, Ghonim M. Role of diffusion-weighted MR imaging in assessing malignant versus benign skull-base lesions. Radiol Med (Torino) 2011;116(1):125–132
19 White ML, Zhang Y, Robinson RA. Evaluating tumors and tumor-like lesions of the nasal cavity, the paranasal sinuses, and the adjacent skull base with diffusion-weighted MRI. J Comput Assist Tomogr 2006;30(3):490–495
20 Ginat DT, Mangla R, Yeaney G, Johnson M, Ekholm S. Diffusion-weighted imaging for differentiating benign from malignant skull lesions and correlation with cell density. AJR Am J Roentgenol 2012;198(6):W597–W601
21 Le Bihan D, Breton E, Lallemand D, Grenier P, Cabanis E, Laval-Jeantet M. MR imaging of intravoxel incoherent motions: application to diffusion and perfusion in neurologic disorders. Radiology 1986;161(2):401–407
22 Sugahara T, Korogi Y, Kochi M, et al. Usefulness of diffusion-weighted MRI with echo-planar technique in the evaluation of cellularity in gliomas. J Magn Reson Imaging 1999;9(1): 53–60
23 Yeom KW, Lober RM, Mobley BC, et al. Diffusion-weighted MRI: distinction of skull base chordoma from chondrosarcoma. AJNR Am J Neuroradiol 2013;34(5):1056–1061, S1
24 Freeze BS, Glastonbury CM. Differentiation of skull base chordomas from chondrosarcomas by diffusion-weighted MRI. AJNR Am J Neuroradiol 2013;34(10):E113
25 Müller U, Kubik-Huch RA, Ares C, et al. Is there a role for conventional MRI and MR diffusion-weighted imaging for distinction of skull base chordoma and chondrosarcoma? Acta Radiol 2016;57(2):225–232
26 Jian BJ, Bloch OG, Yang I, et al. Adjuvant radiation therapy and chondroid chordoma subtype are associated with a lower tumor recurrence rate of cranial chordoma. J Neurooncol 2010;98(1): 101–108